Energy Fuels **2010,** *24,* 3898–3905 · DOI:10.1021/ef100452c
Published on Web 06/15/2010

energy&fuels
article

Laminar Burning Velocities of 2,5-Dimethylfuran Compared with Ethanol and Gasoline

Guohong Tian,[†] Ritchie Daniel,[†] Haiying Li,[†] Hongming Xu,*[,†] Shijing Shuai,[‡] and Paul Richards[§]

[†]*School of Mechanical Engineering, University of Birmingham, Birmingham, B15 2TT, U.K.,* [‡]*State Key Laboratory of Automotive Safety and Energy, Tsinghua University, Beijing, 100084, China, and* [§]*Innospec Ltd., Innospec Manufacturing Park, Oil Sites Road, Ellesmere Port, Cheshire, CH65 4EY, U.K.*

Received April 10, 2010. Revised Manuscript Received May 17, 2010

The 2,5-dimethylfuran (DMF) has attracted renewed global interest since its improved production methods were published in *Nature* and *Science* in 2007. Its high energy density makes it a promising biofuel and a possible alternative to gasoline. Consequently, a series of studies, led by the University of Birmingham, aims to assess the potential of DMF as an automotive energy carrier. These studies will include an analysis of the spray properties, the laminar flame characteristics, the engine performance, and the subsequent emissions. This paper examines the laminar flame characteristics from a quiescent homogeneous air−fuel mixture. The experiments were conducted using a constant volume vessel and were recorded by high speed schlieren visualization. By measurement of the flame growth following ignition, the laminar flame speed was determined. The calculation of flame stretch yielded the Markstein lengths and the laminar burning velocities. This paper presents the results of DMF combustion for a range of equivalence ratios (0.6−2.0) and initial temperatures (50−100 °C). The flame performance when using DMF is compared to EN228 gasoline and to the most commonly used biofuel substitute for gasoline, ethanol. The data shows that ethanol has the highest laminar burning velocity, followed by gasoline, and then DMF. In the 0.9−1.1 equivalence ratio range, the laminar burning velocity of DMF was very similar to gasoline and the difference was within 10%.

1. Introduction

Faced with the concern on the use of petroleum fuels, there is an urgent need for a medium-term solution to the global fuel supply with respect to environment protection. Until carbon-free power sources become feasible, biofuels can help to address this challenge. Currently, ethanol is the market leading gasoline-alternative; in Brazil, it is now considered price-competitive and has been responsible for significant improvements to the air quality in the last 15 years.[1] However, ethanol has its limitations; it tends to corrode the fuel system and suffers from a low energy density in addition to its high energy consumption in production.[2]

Recently, significant breakthroughs in the mass production technology of 2,5-dimethylfuran (DMF) have been reported.[3] It was claimed that scientists at the University of Wisconsin-Madison had efficiently produced exceptionally high yields of DMF from fructose using a new catalytic biomass-to-liquid process. This discovery promotes the attraction of DMF as a biomass-derived alternative to gasoline.[4−6]

Compared with ethanol, DMF has several advantages. First, its energy density (30 MJ/L) is much closer to gasoline (31.9 MJ/L) and 40% higher than ethanol (21.3 MJ/L, all in low heating value). Second, it has a higher boiling point (92−94 °C) than ethanol (78 °C), which makes it less volatile and more practical as a liquid fuel for transportation.[7] Third, unlike ethanol, DMF is insoluble in water, which makes it stable in storage.[5] More attractively, DMF consumes only one-third of the energy in its production, compared with that required by fermentation for ethanol.[5] In fact, the catalytic strategy successfully developed for the production of DMF from building blocks of fructose or glucose has made the large scale and low-cost production of DMF possible.[6,8] Coupled with the aforementioned improved production techniques, these physicochemical properties make DMF a very promising gasoline alternative. Our own work as world pioneering experimental study of DMF in SI engines has confirmed that without any modification to the engine, DMF can be used as a neat fuel with the engine performance and emissions very similar to the case of gasoline.[9]

The technology used to produce DMF has benefitted from such a high level of research and development that it now asserts a paradigm shift for the renewable energy and chemical industries.[7] This promotes DMF's potential to compete with

*To whom correspondence should be addressed. E-mail: h.m.xu@bham.ac.uk.

(1) Goldemberg, J. The challenge of biofuels. *Energy Environ. Sci.* **2008**, *1*, 523–525.
(2) Inderwildi, O. R.; King, D. A. Quo vadis biofuels? *Energy Environ. Sci.* **2009**, *2*, 343–346.
(3) Dumesic, J. A., Roman-Leshkov, Y. Chheda, J. N. Catalytic Process for Producing Furan Derivatives from Carbohydrates in a Biphasic Reactor. International Patent WO 2007/146636 A1, December 21, 2007.
(4) Luque, R.; Herrero-Davila, L.; Campelo, J. M.; Clark, J. H.; Hidalgo, J. M.; Luna, D.; Marinasa, J. M.; Romeroa, A. A. Biofuels: a technological perspective. *Energy Environ. Sci.* **2008**, *1*, 542–564.
(5) Roman-Leshkov, Y.; Barrett, C. J.; Liu, Z. Y.; Dumesic, J. A. Production of dimethylfuran for liquid fuels from biomass-derived carbohydrates. *Nature* **2007**, *447* (7147), 982.
(6) Zhao, H.; Holladay, J. E.; Brown, H.; Zhang, Z. C. Metal Chlorides in Ionic Liquid Sovlents Convert Sugars to 5-Hydroxymethylfuran. *Science* **2007**, *5831*, 1597–1600.
(7) Binder, J. B.; Raines, R. T. Simple Chemical Transformation of Lignocellulosic Biomass into Furans for Fuels and Chemicals. *J. Am. Chem. Soc.* **2009**, *131* (5), 1979–1985.
(8) Mascal, M.; Nikitin, E. B. Direct, High-Yield Conversion of Cellulose into Biofuel. *Angew. Chem., Int. Ed.* **2008**, *47* (41), 7924–7926.
(9) Zhong, S.; Daniel, R.; Xu, H.; Zhang, J.; Turner, D.; Wyszynski, M. L. Combustion and Emissions of 2,5-Dimethylfuran in a Direct Injection Spark-Ignition Engine. *Energy Fuels* **2010**, *24* (5), 2891–2899.

ethanol and other gasoline-like fuels and demonstrates the urgency to investigate the outstanding issues. As part of a series of investigations, the experimental work in this paper analyzes the laminar flame characteristics which are necessary for improving understanding of its combustion behaviors in engines.

The laminar burning velocity can be used to develop sophisticated numerical combustion models, and these models are essential to the engine development process which involves very complex phenomena.[10] For phenomenological combustion models, a complete knowledge of the chemical kinetics of flame reactions is required.[11] However, because of the complexity and stochastic nature of turbulence, most numerical models rely on the experimental laminar burning velocity to interpret the turbulent component.[12,13] In fact, the laminar burning velocity directly affects the burn rate and thus the engine performance. High burning rates are usually desirable but may cause excessive combustion pressures and temperatures, whereas low rates are uneconomical.[11] The laminar burning velocity can be studied from a quiescent homogeneous mixture, such as that in a constant volume vessel.

The laminar burning velocity is a strong function of the initial temperature and a weak function of pressure.[14] Kurata et al. measured the burning velocity of methane−air mixtures at different initial temperatures and pressures[15] and concluded that the burning velocity was highly dependent on the temperature but not so on pressure. This is reinforced by Jerzembeck and Peters[16] at elevated pressures (1.0−2.5 MPa). The laminar burning velocity also depends on the equivalence ratio and the composition of the residual unburned gas, decreasing linearly with residual fraction.[17−21]

Abundant studies have also been carried out into the variation with fuel type. Bradley and his colleagues investigated the laminar flame propagation with different fuels while developing the laminar flame theory. Their experiments at elevated temperatures and low pressures (up to 1.4 MPa) discovered that ethanol's burning velocity was higher than gasoline's.[22−25] Beeckmann et al. investigated the laminar burning velocity of iso-octane, methanol, and ethanol at elevated pressures and temperatures.[26,27] They also developed a numerical approach to their experiments whereby initial results showed good agreement. Rohl et al. produced close approximations to the laminar burning velocities of pure ethanol and E10 (10% ethanol and 90% gasoline by volume). Their data suggested that the influence of adding 10% ethanol to gasoline is relatively small (< 2% laminar burning velocity variation at stoichiometry).[27] Ilbas et al. measured the laminar burning velocities of hydrogen−air and hydrogen−methane−air mixtures using different blending ratios.[28] They found that the addition of hydrogen promoted flame stability, the ignitable range, and the burning velocity.

For the new gasoline-alternative candidate DMF, little can be found on its laminar flame properties except for the publication by Wu et al.[29,30] Their experiments measured the burning velocities and Markstein lengths with CO_2 and N_2 dilution (up to 15%) at 393 K and atmospheric pressure. They claimed that the dilution ratio increased the flame stability but decreased the laminar burning velocity. So far, the flame characteristics of DMF combustion have not been compared to other fuels in terms of its laminar burning velocity under identical experimental conditions.

This paper reports the benchmarking of DMF against gasoline and ethanol at different initial temperatures. It forms part of a series of experiments to explore the use of DMF as a fuel for automotive applications. Other studies in parallel are underway and will include the fuel spray behavior, the engine performance, and the regulated and unregulated exhaust emissions. The schlieren method[31,32] was used for the laminar flame visualization whereby the burning velocity was

(10) Teraji, A.; Tsuda, T.; Noda, T.; Kubo, M.; Itoh, T. Development of a Novel Flame Propagation Model (UCFM: Universal Coherent Flamelet Model) for SI Engines and Its Application to Knocking Prediction. Document No. SAE 2005-01-0199, 2005.
(11) Fenton, J. *Gasoline Engine Analysis*; Mechanical Engineering Publications: London, U.K., 1986.
(12) Ohyagi, S., Harigaya, Y., Kakizaki, K. Toda, F. *Estimation of Flame Propagation in Spark-Ignition Engine by Using Turbulent Burning Model*, http://www.jsme.or.jp/esd/COMODIA-Procs/Data/001/C85_P503.pdf, January 18, 2010
(13) Stone, R. *Introduction to Internal Combustion Engines*; Macmillan: Basingstoke, U.K., 1985.
(14) Ferguson, C. R. *Internal Combustion Engines: Applied Thermosciences*; Wiley: New York, 1986.
(15) Kurata, O., Takahashi, S. Uchiyama, Y. Influence of preheat temperature on the laminar burning velocity of methane-air mixtures. Document No. SAE 942037, 1994.
(16) Jerzembeck, S.; Peters, N. Measurements of Laminar Flame Velocity and Markstein Length for Standard Gasoline and a Corresponding Reference Fuel Mixture (PRF87). Document No. SAE 2007-01-2006, 2007.
(17) Hu, E.; Huang, Z.; Zheng, J.; Li, Q.; He, J. Numerical study on laminar burning velocity and NO formation of premixed methane−hydrogen−air flames. *Int. J. Hydrogen Energy* **2009**, *34*, 6545–6557.
(18) Kwon, H., Min, K. Laminar Flame Speed Characteristics and Combustion Simulation of Synthetic Gas Fueled SI Engine. Document No. SAE 2008-01-0965, 2008.
(19) Miao, H.; Jiao, Q.; Huang, Z.; Jiang, D. Measurement of laminar burning velocities and Markstein lengths of diluted hydrogen-enriched natural gas. *Int. J. Hydrogen Energy* **2009**, *34*, 507–518.
(20) Ulinski, M.; Moore, P.; Elia, M.; Metghalchi, M. *Laminar burning velocity of methane-air-diluent mixtures*. http://www.mae.cornell.edu/pdf/mu25/ulinski1.pdf
(21) Verhelst, S.; Woolley, R.; Lawes, M.; Sierens, R. Laminar and unstable burning velocities and Markstein lengths of hydrogen−air mixtures at engine-like conditions. *Proc. Combust. Inst.* **2005**, *30*, 209–216.
(22) Bradley, D.; Lawes, M.; Mansour, M. S. Explosion bomb measurements of ethanol−air laminar gaseous flame characteristics at pressures up to 1.4 MPa. *Combust. Flame* **2009**, *156* (7), 1462.
(23) Bradley, D.; Gaskell, P. H.; Gu, X. J. Burning Velocities, Markstein Lengths, and Flame Quenching for Spherical Methane-Air Flames: A Computational Study. *Combust. Flame* **1996**, *104*, 176–198.
(24) Bradley, D.; Hicks, R. A.; Lawes, M.; Sheppard, C. G. W.; Woolley, R. The Measurement of Laminar Burning Velocities and Markstein Numbers for Iso-octane−Air and Iso-octane−n-Heptane−Air Mixtures at Elevated Temperatures and Pressures in an Explosion Bomb. *Combust. Flame* **1998**, *115*, 126–144.
(25) Gu, X. J.; Haq, M. Z.; Lawes, M.; Woolley, R. Laminar Burning Velocity and Markstein Lengths of Methane−Air Mixtures. *Combust. Flame* **2000**, *121*, 41–58.
(26) Beeckmann, J.; Röhl, O.; Peters, N. Experimental and Numerical Investigation of Iso-Octane, Methanol and Ethanol Regarding Laminar Burning Velocity at Elevated Pressure and Temperature. Document No. SAE 2009-01-1774, 2009.
(27) Röhl, O.; Jerzembeck, S.; Beeckmann, J.; Peters, N. Numerical Investigation of Laminar Burning Velocities of High Octane Fuel Blends Containing Ethanol. Document No. SAE 2009-01-0935, 2009.
(28) Ilbas, M.; Crayford, A. P.; Yílmaz, I.; Bowen, P. J.; Syred, N. Laminar-burning velocities of hydrogen−air and hydrogen−methane−air mixtures: An experimental study. *Int. J. Hydrogen Energy* **2006**, *31*, 1768–1779.
(29) Wu, X.; Huang, Z.; Jin, C. Measurements of Laminar Burning Velocities and Markstein Lengths of 2,5-Dimethylfuran-Air-Diluent Premixed Flames. *Energy Fuels* **2009**, *23*, 4355–4362.
(30) Xuesong, W.; Zuohua, H.; Tao, Y. Identification of combustion intermediates in a low-pressure premixed laminar 2−5-dimethylfuran-oxygen-argon flames with tunable synchrotron photoionization. *Combust. Flame* **2009**, *156* (7), 1365–1376.
(31) Settles, G. S., Ed. *Schlieren and Shadowgraph Techniques: Visualizing Phenomena in Transparent Media*; Springer: Berlin, Germany, 2001.
(32) Pastor, J. V.; García, J. M.; Pastor, J. M.; Zapata, L. D. Evaporating Diesel Spray Visualization using a Double-pass Shadowgraphy/Schlieren Imaging. Document No. SAE 2007-24-0026, 2007.

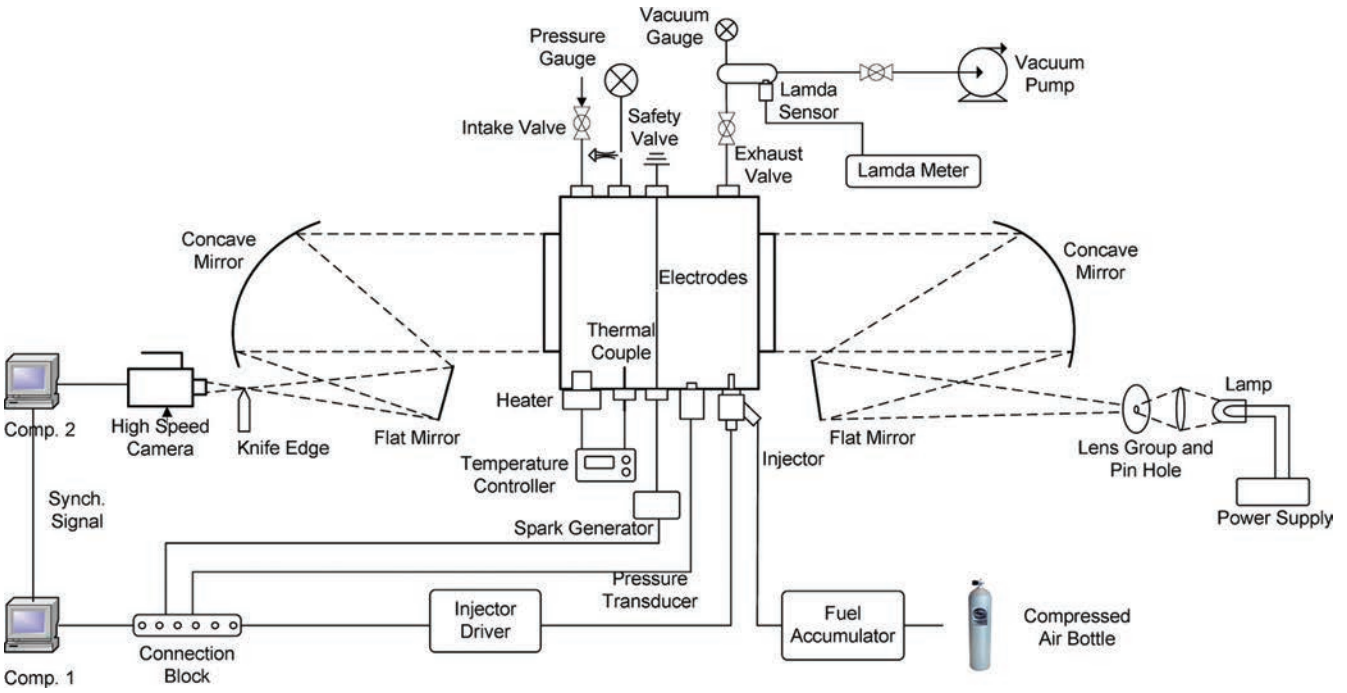

Figure 1. Schematic diagram of the experimental setup.

calculated from in-house image processing code. The experimental setup is described in the next section and the results from these experiments are then presented and discussed, with conclusions drawn at the end of the paper.

2. Experimental Facilities and Program

2.1. Experimental Setup. Figure 1 shows the experimental system layout. The tests were carried out under 0.1 MPa initial pressure and three different initial temperatures (50, 75, and 100 °C).

A constant volume vessel, with two opposing circular windows (100 mm diameter, fused silica), was used for the experiments. Heating coils were secured to each corner of the vessel walls to heat the vessel evenly. The interior air temperature was controlled using a closed-loop feedback controller. A pair of tungsten electrodes, 1 mm in diameter and 1 mm apart, was used to initiate the spark. The discharge energy can be adjusted by varying the TTL control signal width, which for all the experiments was fixed to 10 ms. For safety reasons, a pressure release valve was installed and set to 0.7 MPa.

A 500 W xenon lamp was used as the light source. The light was focused onto a pinhole using a group of lenses in order to generate the spotlight for the schlieren method. Passing through a series of mirrors, the light path was then cut using a knife-edge, which is essential for the schlieren technique.[31] A Phantom V7.1 high-speed camera then captured the schlieren images; at the highest resolution (800 × 600 pixels), 6600 pictures can be captured every second. The camera was synchronized with the spark timing and the interior pressure rise recording. After performance matching, the sample rate was set to 3 kHz.

For each test, the vessel was scavenged and evacuated to 10 kPa absolute pressure, and the fuel was injected into the vessel with good atomization using a multihole gasoline direct injection (GDI) injector at an injection pressure of 10 MPa. The injected fuel mass was precisely controlled by injection duration using precalibrated data. The vapor pressures of the three fuels at the initial temperatures are listed in Table 1 and the different partial pressures with increasing equivalence ratio have been calculated for a mixture pressure of 0.1 MPa, given in Figure 2. It is shown that the partial pressures for the three fuels at each test condition are lower than their corresponding vapor pressure. This guarantees full evaporation from 50 to 100 °C.

Table 1. Vapor Pressures of the Fuel Candidates (kPa)

fuel\temperature	50 °C	75 °C	100 °C
gasoline[33a]	147.5	272.6	464.0
DMF[34]	20.3	54.7	126.3
ethanol[12,35b]	29.5	88.8	225.7

[a] The Reid vapor pressure (RVP) for gasoline is calculated according to the cited reference based on the specification given by the fuel supplier. [b] Calculated by the online calculator and online database.

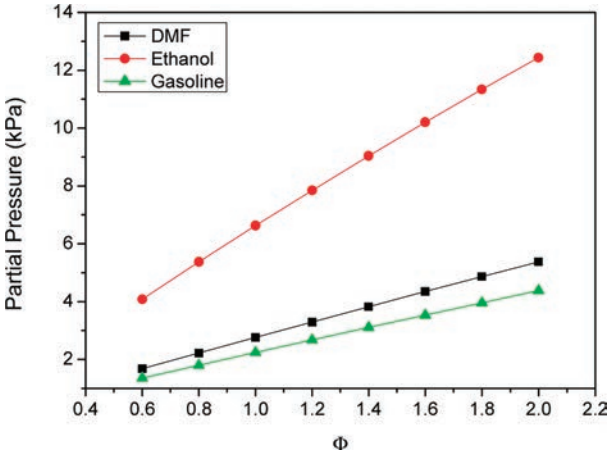

Figure 2. Variations of partial pressure of the tested fuels with equivalence ratio.

The intake valve was opened after the fuel was fully vaporized, and fresh air was introduced into the vessel until ambient pressure was restored. After 5 min of quiescence to allow for the homogeneous mixing of fuel and air, the mixture was ignited. This triggered the high-speed camera and data logging system, which in turn recorded the schlieren images and pressures. To validate the equivalence ratio, the burned gas was captured in a sealed chamber and measured using an ETAS LA4 lambda meter. The measured equivalence ratio was then compared with

the calculated values and they showed good agreement. For each of the testing points, three measurements were carried out for checking repeatability.

2.2. Data Processing. An in-house MATLAB code was used to process the images and determine the burning velocity automatically. To avoid the impact of flame quenching from the electrodes, the spherical flame front was measured in the vertical direction by detecting the density change between the burned and unburned gas (see Figure 3). Furthermore, to avoid the influence of ignition energy at the beginning and the rise of pressure at the end, the analyzed observation region was focused only on the flame front radii between 6 and 18 mm from the electrode, in the method widely adopted, e.g., by other researchers.[22−25,36].

Despite not being the same as the cold flame radius,[24] the schlieren image radius is commonly used in calculations of flame speed.[29,31] Therefore, in order to determine the stretched laminar flame speed, S_n, the time dependent flame front radii changes (r_u) are measured from these schlieren images by

$$S_n = \frac{dr_u}{dt} \quad (1)$$

where r_u is the flame front radius. For the outwardly propagating flame, with known stretched laminar flame speed and radius, the stretch rate, α, can be determined:[24,25]

$$\alpha = \frac{d(\ln A)}{dt} = \frac{1}{A}\frac{dA}{dt} = \frac{2}{r_u}S_n \quad (2)$$

where A is the spherical flame surface area ($4\pi r_u^2$). At the early stage of flame propagation, there is a linear relationship between the stretch rate and flame speed:[24,25]

$$S_n = S_s - (L_b\alpha) \quad (3)$$

where S_s is the unstretched flame speed and L_b is the Markstein length. S_s and L_b are determined by extrapolating S_n to the zero stretch rate and by measuring the gradient of this line, respectively. The unstretched laminar burning velocity u_l is then deduced from S_s:[24,25]

$$u_l = S_s\frac{\rho_b}{\rho_u} \quad (4)$$

Assuming the pressure is constant, the burned (ρ_b) and unburned gas densities (ρ_u) can be found from the conservation of mass equation:

$$\frac{\rho_b}{\rho_u} = \frac{V_u}{V_b} = \frac{n_u T_u}{n_b T_b} \quad (5)$$

n_u, n_b = mole numbers of reactants and products and T_u, T_b = initial and adiabatic flame temperatures. The adiabatic flame temperatures were calculated using HPFLAME,[37] which incorporates the Olikara and Borman equilibrium routines.[38]

3. Results and Discussion

3.1. Spherical Flame Morphology. Three typical schlieren images for the three fuels at stoichiometric conditions and at an initial temperature of 75 °C are juxtaposed in Figure 4. The time elapsed from the point of ignition is shown.

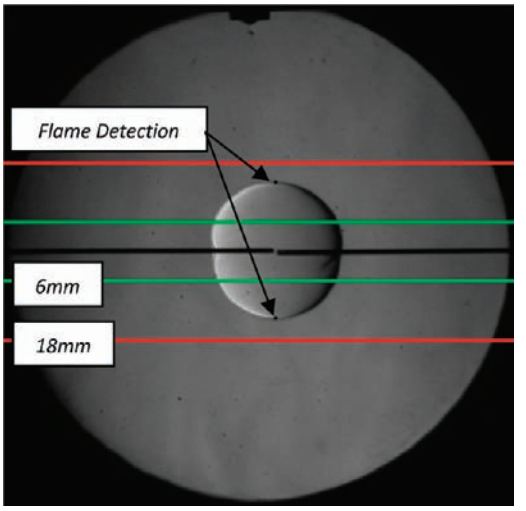

Figure 3. A sample schlieren image showing the region of analysis.

The flame speed of ethanol is clearly the highest; the advanced flame front, which is established after 3 ms, is maintained throughout the expansion. Clearly, the difference between the cases of DMF and gasoline is very small.

It appears that the initiation of the gasoline flame shown in Figure 4 has been effected by the spark energy at the start of combustion. Therefore, the influence of the spark instability can be ignored by restricting the observation region to the radii greater than 6 mm (up to 18 mm),[23,36] and the flame radius in the vertical direction is used in the analysis in this study.

The DMF flame propagates evenly in all radial directions; the surface appears smooth and therefore stable. However, as with the other flames, slight wrinkling is observed near the electrode due to the quenching effect, but this does not affect the overall shape. When the spherical flame approaches the edge of the window, the shape becomes distorted. This effect can be observed more clearly on the ethanol flame after 15 ms, as it has reached the most advanced stage. The flame's shape becomes more oval with flatter vertical surfaces. This was believed to be related to the instability of buoyancy and the influence of the internal geometry of the combustion chamber.[24,39] Also from the ethanol flame images, a slight crack is observed after 5 ms, which might be caused by the quenching effect of the electrodes.

3.2. Flame Propagation Speed and Markstein Length. *Stretched Flame Speed.* The stretched flame speed is described as the rate of change of the schlieren flame radius (see eq 1). In this work, the effect of the spark energy on the flame speed is isolated and the flame speed is measured between the distances of 6 and 18 mm from the center point of ignition. For each test, the traversed distance of the top and bottom flame front locations was deduced using the MATLAB code, as illustrated by Figure 3.

Figure 5 shows the measured stretched flame speeds with respect to the stretch rate for the three test fuels at an initial temperature of 75 °C. With respect to time, the points move toward the zero stretch rate. Through linear extrapolation, the unstretched flame speed S_s can be determined at the zero

(33) *Evaporation Loss from Internal Floating Roof Tanks*, 3rd ed.; Bulletin No. 2519, American Petroleum Institute: Washington, DC, 1982.
(34) Yaws, C. L. *Yaws' Handbook of Thermodynamic and Physical Properties of Chemical Compounds: Physical, Thermodynamic and Transport Properties for 5,000 Organic Chemical Compounds*; Knovel: Norwich, NY, 2003.
(35) Ohe, S. Computer Aided Data Book of Vapor Pressure. http://e-data.jp/vpcal2/e/ (Accessed July 12, 2009).
(36) Chen, Z.; Burke, M. P.; Ju, Y. Effects of Lewis number and ignition energy on the determination of laminar flame speed using propagating spherical flames. *Proc. Combust. Inst.* **2009**, *32*, 1253–1260.
(37) Turns, S. R. *An Introduction to Combustion*; McGraw-Hill: New York, 1996; pp 55−56.
(38) Olikara, C.; Borman, G. L. A Computer Program for Calculating Properties of Equilibrium Combustion Products with Some Applications to I. C. Engines. Document No. SAE 750468, 1975.
(39) Law, C. K.; Sung, C. J. Structure, aerodynamics, and geometry of premixed flamelets. *Prog. Energy Combust. Sci.* **2000**, *26*, 459–505.

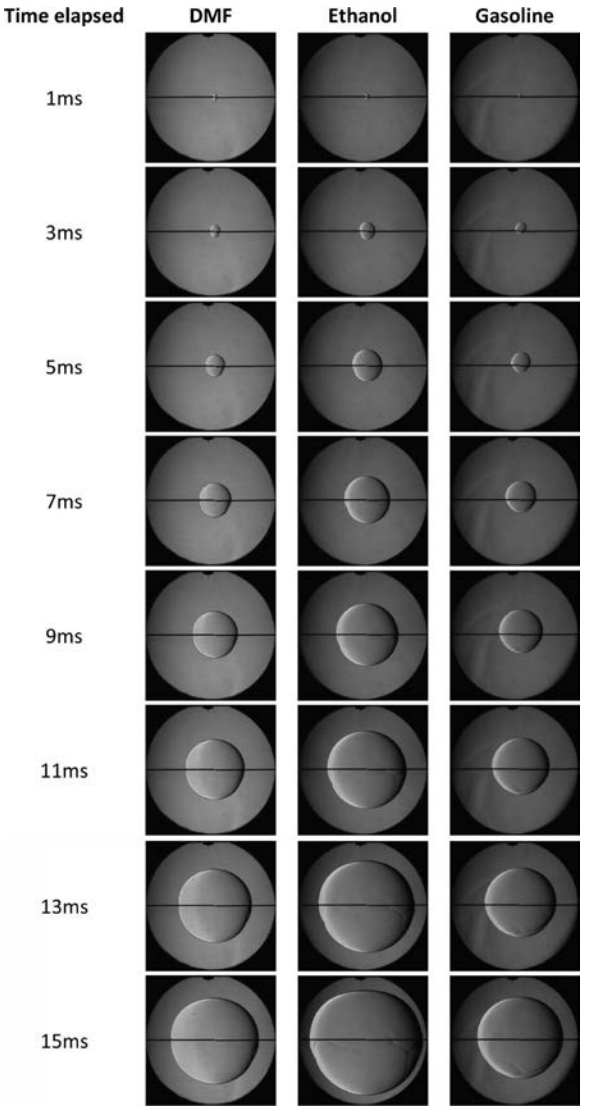

Figure 4. Chronological schlieren images for the tested fuels at the stoichoimetric equivalence ratio and an initial temperature of 75 °C.

stretch rate and the Markstein length, L_b, using the gradient of the line. Because of the inverse proportionality between the flame stretch rate and flame radius (see eq 2), the flame stretch rate is the highest at small radii. As the flame size grows and approaches the 18 mm radius point, the rate of stretch rate change reduces and the line becomes nonlinear, which is shown in Figure 5. Beyond this point, the flame is affected by the shape of the chamber and the combustion pressure rise. It must be noted that the choice of the upper limit for the flame sizes influences the results to be calculated, and the method using extrapolation to zero stretch is the most widely adopted boundary condition[22−25,29,30] in despite of its limitation. This method has been used in the present study in order to enable a comparison with the existing related information in the literature.

Unstretched Flame Speed. With the stretched flame speeds analyzed, it is now possible to determine the unstretched flame speeds for each of the three fuels. These can be found using the linearly fitted line of stretched flame speed against stretch rate by extending the lines to the zero stretch. The results for each of the initial temperatures (50, 75, and 100 °C) are shown in Figure 6.

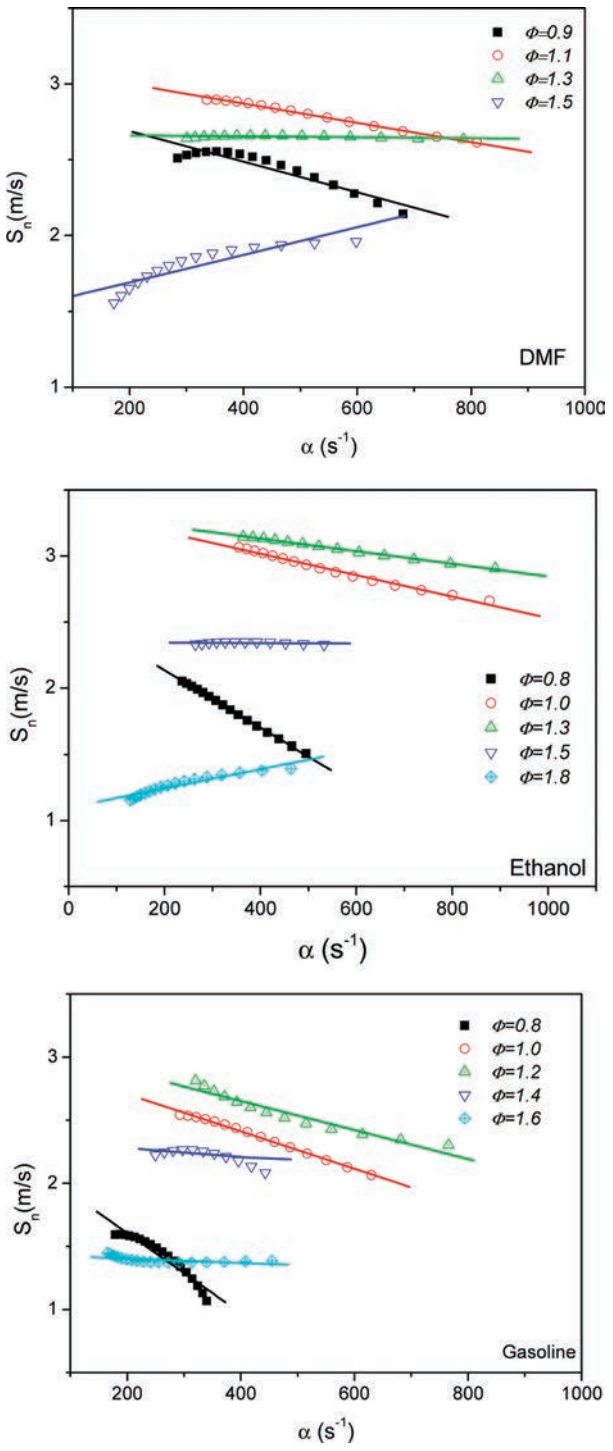

Figure 5. Stretched flame speed of the tested fuels at an initial temperature of 75 °C for different equivalence ratios and stretch rates.

For the three tested fuels, the fastest flame propagation occurred in the slightly rich mixtures when the equivalence ratio was between 1.0 and 1.2, as expected. At 50 °C, ethanol had the highest unstretched flame speed, which was followed by DMF and then gasoline. In fact, the DMF and gasoline results are very similar, whose relationship continues with rising temperature. The ethanol flame is also seen to yield the highest speeds for 75 and 100 °C throughout the fuel−air mixture range.

Markstein Length. The burning gas Markstein length, L_b, is the negative of the slope of the linearly fitted line of

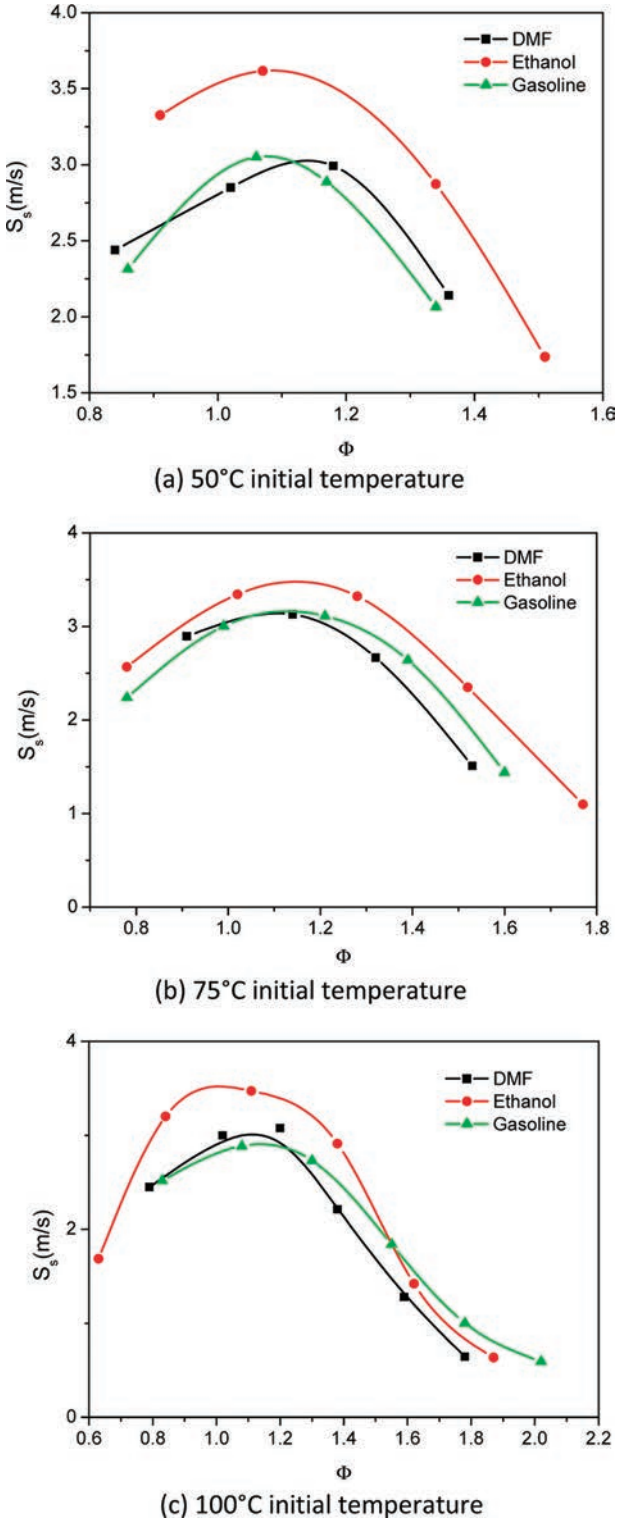

Figure 6. Unstretched flame speed of the tested fuels at different initial temperatures and equivalence ratios.

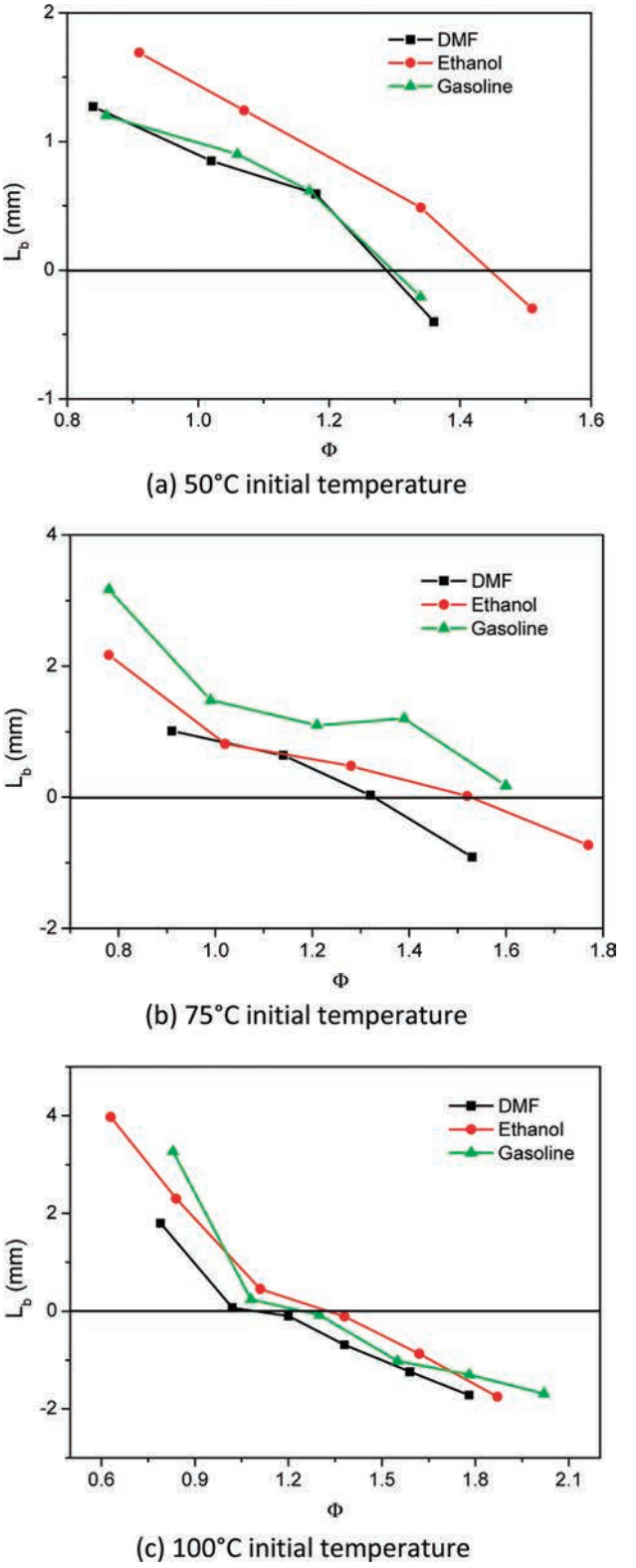

Figure 7. Markstein length of tested fuels at different initial temperatures and equivalence ratios.

stretched flame speed against stretch rate (see Figure 5). It indicates the influence of stretch rate on the flame propagation speed and characterizes the flame instability.[39,40] Positive Markstein lengths indicate that the flame speed is decreased with the increase of the stretch rate, while a negative Markstein length indicates that the flame speed is increased with the increase of the stretch. According to Bradley et al.,[24] if the Markstein number exceeds 1.5, the flame is initially stable until a critical flame radius is reached.

Figure 7 shows the Markstein lengths for all the three fuels under their different test conditions. Generally, the Markstein lengths decrease with increasing equivalence ratio for each initial temperature. This is because all the tested fuels are heavy

(40) Bechtold, J. K.; Matalon, M. The Dependence of the Markstein Length on Stoichiometry. *Combust. Flame* **2001**, *127*, 1906–1913.

hydrocarbon−air mixtures, and the Markstein length depends only on the Lewis number of the deficient reactants.[40]

With regards to temperature, the Markstein lengths have higher values at low equivalence ratios (Φ = 0.8−0.9) when the temperature is increased. This suggests the lean flames are more stable at higher temperatures. However, the Markstein lengths then decrease more rapidly from these higher values suggesting the stability quickly decays. This is also shown by the earlier entry at higher temperatures into negative Martkstein lengths with respect to the equivalence ratio for all three fuels. This indicates that at higher temperatures, the flame is more susceptible to accelerate with increasing stretch rate. The rapid decay results in lower Markstein lengths at rich equivalence ratios.

With the exception of 75 °C, the ethanol flame appears to be the most stable through the entire range of air−fuel mixtures. However, the difference is not significant. The DMF flame, on the other hand, is always below the ethanol flame and partly so for the gasoline flame for this temperature range. This suggests that the DMF flame is slightly more unstable.

It is noticed that the ranking of the fuels in terms of Markstein length for given equivalence ratio changes with temperature. Indeed, the influence of temperature on Markstein length for different fuels is still unclear. Therefore it is difficult to discuss the ranking of fuels under different initial temperatures and given equivalence ratio. This paper has just shown the measured results whereas more investigations will be needed in order to provide the required explanation.

3.3. Laminar Burning Velocity. One of the key indicators of flame behavior is the laminar burning velocity. This is calculated using the unstretched flame speed and expansion ratio from eqs 4 and 5. The results for the three fuels are shown in Figure 8 for the range of initial temperatures.

It is clear that ethanol has the highest burning velocity among the three fuels for all the initial temperatures. For instance, at 50 °C the peak laminar burning velocity of ethanol (56 cm/s) is 13 cm/s higher than for the gasoline mixture (43 cm/s). This difference increases to 17 cm/s for 75 °C and 15 cm/s for 100 °C. This reinforces ethanol's superiority in terms of laminar burning velocity. These velocities are higher than the results from the research group in Aachen,[26,27] as expected, where the measurement was taken at lower initial pressures. However, they agree well with those results from Egolfopoulos et al.[41]

For the other two fuels, gasoline's laminar burning velocity is more closely matched by DMF, although the laminar burning velocity of DMF is marginally lower. The difference increases as temperature increases and equivalence ratios rise above 1.2. Nevertheless, their profiles are very similar and the curvature is less significant than for ethanol. In real-world engineering applications, e.g., for automotive engines, the equivalence ratios will only slightly deviate around stoichiometric conditions (Φ = 0.9−1.2) due to the requirement of the three-way catalyst aftertreatment system to meet emission legislations. In this region the difference between the laminar burning velocity of DMF and gasoline is less than 10%.

Ethanol has shown great potential in fast burn combustion systems in terms of its laminar burning velocity. Although the velocity decreases significantly when the equivalence ratio goes beyond 1.6, the magnitude is very high in the wide range near stoichiometry. The difference between the laminar burning velocity of DMF and ethanol in the typical engine application region (Φ = 0.9−1.2) is almost 30%.

The curvature of these graphs closely resembles those of other fuels documented by Heywood,[42] under ambient test

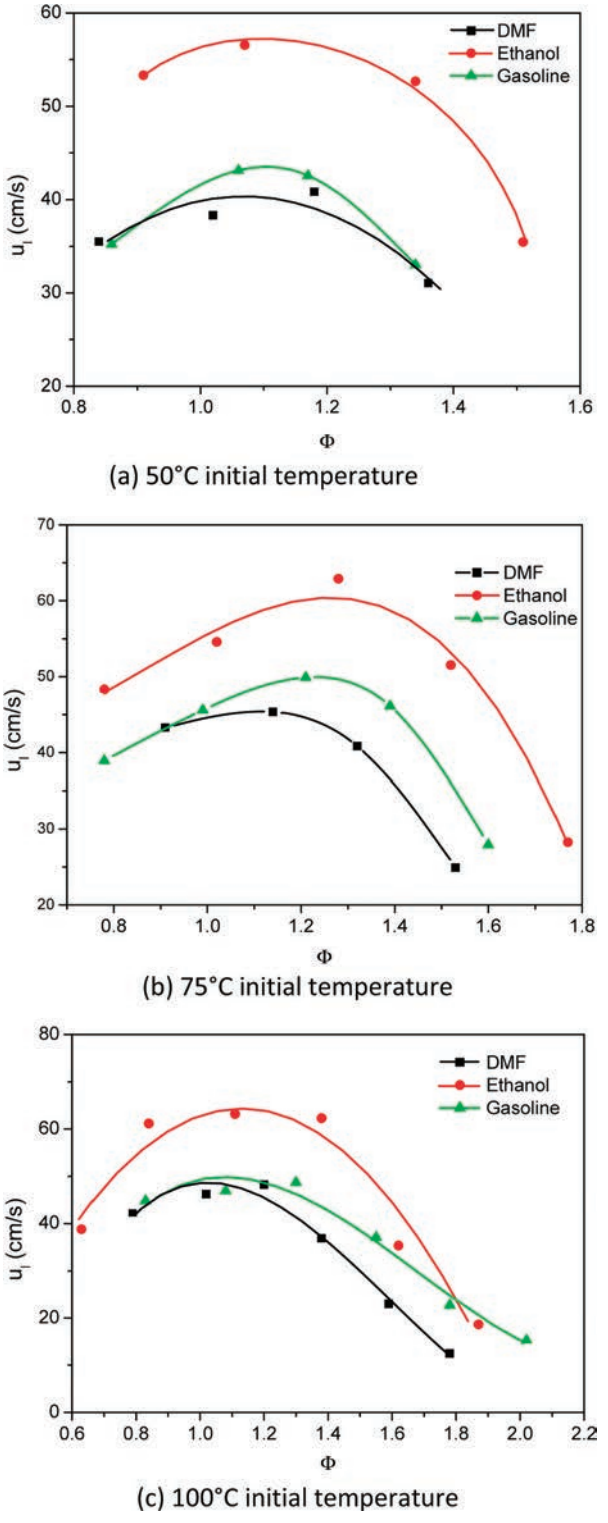

Figure 8. Laminar burning velocity of tested fuels at different initial temperatures and equivalence ratios.

(41) Egolfopoulos, F. N.; Du, D. X.; Law, C. K. A study on ethanol oxidation kinetics in laminar premixed flames, flow reactors, and shock tubes. *Symp. (Int.) Combust.* **1992**, *24* (1), 833–841.

(42) Heywood, J. B. *Internal Combustion Engine Fundamentals*; McGraw-Hill: New York, 1988.

conditions with respect to temperature and pressure, where the peak laminar burning velocity of gasoline at 27 °C is given as 36 cm/s. In our tests, at 50 °C the peak is 44 cm/s, an increase of 8 cm/s. This highlights how the initial temperature affects the burning velocity. Increasing the temperature from 50 to 100 °C brings the peak velocities of gasoline from 44 cm/s further to 50 cm/s. For DMF and ethanol, when the initial temperature increased for 50 °C, the peak velocities increased from 40 and 56 cm/s to 49 and 64 cm/s, respectively. It also appears to bring the burning velocity for the other equivalence ratios up. For instance, when the temperature was doubled from 50 to 100 °C, the differences between the surrounding equivalence ratio points are reduced. The results by Wu et al.[29] suggest that DMF's laminar burning velocity can exceed this. Their tests at a similar pressure but higher temperature (120 °C) suggest that at an equivalence ratio of 1.2, the velocity can reach 55 cm/s.

It must be noted that measuring the burning velocity of different fuels as such is subject to some uncertainty in relation to the experimental system setup and data processing. It is recognized that for most fuels, the maximum burning velocity usually occurs at the air−fuel ratio of around 1.1, which was unfortunately not included for all the tests in this investigation, e.g., for ethanol at 75 °C. The drawing of lines over the data points is an indication of the trend but may not be necessarily representing the missing data. In general, however, the results of the present study are consistent with the findings mentioned above when the difference in the test condition is considered, and the trend of the data is as indicative as the existing information in literature for other fuels.[42]

4. Conclusions

An experimental investigation into the flame propagation characteristics of 2,5-dimethylfuran (DMF) were performed using the schlieren optical method. All the tests were conducted at ambient pressure but with varying initial temperature (50, 75, and 100 °C) and equivalence ratio (Φ = 0.6−2.0). The performance of the DMF flames were benchmarked against gasoline and compared to ethanol. The conclusions are summarized as follows: (1) For the three fuels, the highest stretched flame speeds occurred between the equivalence ratios of 1.1 and 1.3. (2) There is a marginal difference in flame stability between the three fuels. This was shown by the similarities between the Markstein lengths of the tested fuels. (3) The laminar burning velocity of DMF is closer to gasoline than ethanol for given initial test conditions. However, ethanol's laminar burning velocity is the highest among the three fuels for the test conditions studied with respect to temperature and equivalence ratio, and it is approximately 30−40% faster compared with DMF. The laminar burning velocity of gasoline is slightly faster than that of DMF (less than by 10% in the region of 0.9−1.1 equivalence ratio).

Acknowledgment. The present work is part of a 3 year research project sponsored by the Engineering and Physical Sciences Research Council (EPSRC) under Grant EP/F061692/1. The help from the EPSRC Engineering Instrument Pool in relation to the loan and setting up of the high-speed camera is gratefully acknowledged. The authors wish to specially thank Jaguar Land Rover for their support on the test facilities.